Clays and Clay Minerals, Vol. 57, No. 5, 513–520, 2009.

RELATIONSHIP BETWEEN Pb^{2+} ADSORPTION AND AVERAGE Mn OXIDATION STATE IN SYNTHETIC BIRNESSITES

WEI ZHAO, HAOJIE CUI, FAN LIU, WENFENG TAN, AND XIONGHAN FENG*

Key Lab of Subtropical Agriculture Resource and Environment, Ministry of Agriculture, Huazhong Agricultural University, Wuhan, 430070, China

Abstract—The relationship between vacant Mn structural sites in birnessites and heavy-metal adsorption is a current and important research topic. In this study, two series of birnessites with different average oxidation states (AOS) of Mn were synthesized. One birnessite series was prepared in acidic media (49.6−53.6 wt.% Mn) and the other in alkaline media (50.0−56.2 wt.% Mn). Correlations between the Pb^{2+} adsorption capacity and the d_{110} interlayer spacing, the AOS by titration, and the release of Mn^{2+}, H^+, and K^+ during adsorption of Pb^{2+} were investigated. The maximum Pb^{2+} adsorption by the birnessites synthesized in acidic media ranged from 1320 to 2457 mmol/kg with AOS values that ranged from 3.67 to 3.92. For birnessites synthesized in alkaline media, the maximum Pb^{2+} adsorption ranged from 524 to 1814 mmol/kg, with AOS values between 3.49 and 3.89. Birnessite AOS values and Pb^{2+} adsorption increased as the Mn content decreased. The maximum Pb^{2+} adsorption to the synthetic birnessites calculated from a Langmuir fit of the Pb adsorption data was linearly related to AOS. Birnessite AOS was positively correlated to Pb^{2+} adsorption, but negatively correlated to the d_{110} spacing. Vacant Mn structural sites in birnessite increased with AOS and resulted in greater Pb^{2+} adsorption. Birnessite AOS values apparently reflect the quantity of vacant sites which largely account for Pb^{2+} adsorption. Therefore, the Pb^{2+} adsorption capacity of birnessite is mostly determined by the Mn site vacancies, from which Mn^{2+}, H^+, and K^+ released during adsorption were derived.

Key Words—Adsorption, Birnessite, Mn Average Oxidation State, Pb^{2+}, Vacant Mn Structural Site.

INTRODUCTION

Lead is an environmental heavy metal that has always attracted much attention. Examination of the mechanisms that determine Pb and soil-component interactions is crucial to understanding the fate of Pb in soils, sediments, and water. A greater understanding of Pb interaction mechanisms could also help in water purification and in remediation efforts in Pb-contaminated soil (Matocha *et al.*, 2001).

Manganese oxides are extensively distributed in soils, sediments, and ocean Mn nodules. Manganese oxides commonly have a low point of zero charge, large surface area, large negative charge, and are very active in various chemical reactions; they are also considered to be important adsorbents of Pb (McKenzie, 1980; O'Reilly and Hochella, 2003; Post, 1999). The phyllomanganate mineral, birnessite, is the most common type of manganese oxide in soils. Many Mn oxides can be synthesized by direct or indirect transformation of birnessite (Golden *et al.*, 1987; Tu *et al.*, 1994). Birnessites are usually synthesized in acidic or alkaline media using one of two approaches. Firstly, birnessites can be synthesized by the reduction of $KMnO_4$ in a strongly acidic medium (McKenzie, 1971). The resulting birnessite has hexagonal layer symmetry with layers consisting of edge-sharing $Mn(IV)O_6$ octahedra, $Mn(III)O_6$ octahedra, and vacant Mn octahedral sites (Villalobos *et al.*, 2006). Some Mn^{2+} and Mn^{3+} are located above or below vacant Mn octahedral sites in birnessites (Webb *et al.*, 2005). The number of vacant Mn octahedral sites can reach up to 12% (Villalobos *et al.*, 2006). Secondly, birnessites can be synthesized by the oxidation of manganese hydroxide in a strong alkali medium (Luo and Suib, 1997; Villalobos *et al.*, 2003; Feng *et al.*, 2004). In the structure of this synthetic birnessite, Mn^{3+}-rich rows parallel to the *b* axis are separated from one another along the *a* axis by two Mn^{4+} rows (Drits *et al.*, 1997; Lanson *et al.*, 2002a). The amount of vacant Mn octahedral sites can reach up to 5% (Manceau *et al.*, 2002; Post and Veblen, 1990). Birnessite structural vacancies account for a negative layer charge and relate to the adsorption of Pb, Zn, Cu, Cd, and Ni, to the oxidation of Co^{2+} and Cr^{3+}, and to the transformation of minerals (Appelo and Postma, 1999; Burns, 1976; Lanson *et al.*, 2002b; Manceau and Charlet, 1992; Peacock and Sherman, 2007; Villalobos *et al.*, 2006). Surface-adsorbed Pb on birnessite was octahedrally coordinated and ~75% of the Pb was located either above or below vacant Mn sites. The rest of the Pb was located above or below empty tridentate cavities, sharing three edges with neighboring MnO_6 in the layer (Lanson *et al.*, 2002b). A proportion of the Pb forms double-corner-sharing complexes at particle edges of birnessite (Villalobos *et al.*, 2005).

* E-mail address of corresponding author:
fxh73@mail.hzau.edu.cn
DOI: 10.1346/CCMN.2009.0570501

A greater number of vacant sites in a mineral crystal structure would cause unit-cell-parameter (*a* or *b* axis) distortion in some lattice-plane directions. For birnessite, greater numbers of vacant sites would lead to an increase in the repulsive forces between adjacent cations around the vacant sites and the coordinating anions of shared octahedra would tend to be drawn closer or pushed further away. The increased distortion of the crystal structure along (*hk*0) would result in a decrease in (*hk*0) interplanar spacings (Bailey, 1966). Variation in (*hk*0) interplanar spacings could therefore reflect variation in the amount of vacant Mn octahedral sites. Besides H^+, other cations released, such as Mn^{2+} and K^+, might also explain Pb adsorption. An intrinsic relationship should also exist between the total amount of cations released and the amount of heavy metal adsorbed. Clearly, an analysis of the total amounts of individual cations released during adsorption should help in understanding how heavy metals adsorb to birnessites.

The objectives of this study are outlined in the following questions. (1) Pb clearly can be adsorbed above or below vacant sites, but does the quantity of vacant Mn structural sites in birnessite influence the amount of adsorbed Pb^{2+} coordinated to birnessite surfaces? (2) What are the relationships between vacant sites and Mn AOS and between vacant sites and Mn^{2+}, H^+, and K^+ release during the adsorption? (3) What are the relationships among AOS, d_{110} interlayer spacing, and Pb^{2+} adsorption? The results of this study help our understanding of the mechanism of heavy-metal adsorption to birnessites.

MATERIALS AND METHODS

Synthesis of birnessite

In acidic media, birnessite was synthesized according to the method described by McKenzie (1971). Synthetic birnessites designated HB1, HB2, HB3, HB4, HB5, and HB6 were prepared using 45, 53.3, 53.3, 45, and 66.7 mL aliquots, respectively, of 6 M HCl and a 55 mL aliquot of 8 M HCl added dropwise at a rate of 0.7 mL/min to a 0.2 M solution of boiling $KMnO_4$ in 300−400 mL of distilled, deionized water. Vigorous stirring was used during the reaction. After further boiling for 30 min, the products were aged for 12 h at 60ºC (Feng *et al.*, 2007). Birnessites were prepared in alkaline media by the method of Villalobos *et al.* (2003). Synthetic birnessites designated OHB1, OHB2, OHB3, OHB4, OHB5, OHB6, OHB7, and OHB8 were prepared using 125 mL aliquots of 0.364, 0.364, 0.444, 0.444, 0.444, 0.5, and 0.6 M $MnCl_2$, respectively, mixed with 6.3 M KOH in 125 mL of distilled, deionized water to form a pink gel precipitate of $Mn(OH)_2$. A 250 mL aliquot of 0.1 M $KMnO_4$ was added dropwise to the $Mn(OH)_2$ precipitates at a rate of 3 mL/min and stirred vigorously to form dark gray precipitates. The final Mn^{7+}/Mn^{2+} molar ratios used in the reactions were 0.55, 0.55, 0.45, 0.45, 0.45, 0.4, and 0.33. After further stirring for 30 min, the products were aged for 12 h at 60ºC. All of the synthetic birnessites were purified by electrical dialysis at 150−220 V until the conductivities of the supernatants were <20 μS/cm and were then dried at 40ºC.

Characterization

X-ray diffraction (XRD) analyses were performed with a D/Max-3B diffractometer (Rigaku, Japan) using monochromatic FeKα radiation. The diffractometer was operated at a tube voltage of 40 kV and a tube current of 20 mA. For regular analyses, intensities were measured at 10−90º2θ using a count time of 0.2 s/step. For fine analyses, rutile was used as an internal standard and intensities were measured at 83−89º2θ using a count time of 15 s/step. The step intervals were 0.02º2θ.

Transmission electron microscope (TEM) analyses were carried out using a CM 12 (Philips, Netherlands) transmission electron microscope operated at 120 kV. The samples were crushed gently to a powder, dispersed in absolute ethyl alcohol, and dispersed ultrasonically prior to deposition on holey carbon films. High-resolution TEM examination was performed on sample suspensions dried on holey carbon grids using a JEM 2010 FEF (JEOL, Japan) transmission electron microscope operated at 200 kV.

Average oxidation state of Mn

The total Mn contents were determined on 0.1 g samples of the synthetic birnessites dissolved in 25 mL of 0.25 M hydroxylamine hydrochloride diluted to 250 mL. A 1.0 mL aliquot of each dissolved and diluted birnessite sample was diluted to 100 mL and the Mn content determined using an AAS 240FS flame atomic absorption spectrometer (Varian, Australia). The AOS was measured using the oxalic acid-permanganate back-titration method (Kijima *et al.*, 2001). A 0.1 g sample of each birnessite was completely dissolved in 5 mL of 0.5 M $H_2C_2O_4$ and 10 mL of 1 M H_2SO_4 to reduce all the more highly charged Mn ions to Mn^{2+}. Excess $C_2O_4^{2-}$ was determined by back-titration using a standardized 0.02555 M $KMnO_4$ solution at 75ºC. The AOS was calculated based on both the total Mn content and the AOS titration.

Adsorption experiments

Isothermal Pb^{2+} adsorption to the synthetic birnessites was measured using 5 g/L sample suspensions at pH 5.00 and a series of pH 5.00 Pb^{2+} solutions at concentrations ranging from 0 to 15 mmol Pb/L. The ionic strength was adjusted to 0.15 using $NaNO_3$. The pH of the 5 g/L birnessite suspensions was maintained at 5.00±0.05 by the addition of 0.1 M HNO_3 or 0.1 M NaOH. Then, 5 mL aliquots of the birnessite sample suspensions were mixed with 10 mL of Pb^{2+} solutions, with a range of initial concentrations, in 50 mL

https://doi.org/10.1346/CCMN.2009.0570501 Published online by Cambridge University Press

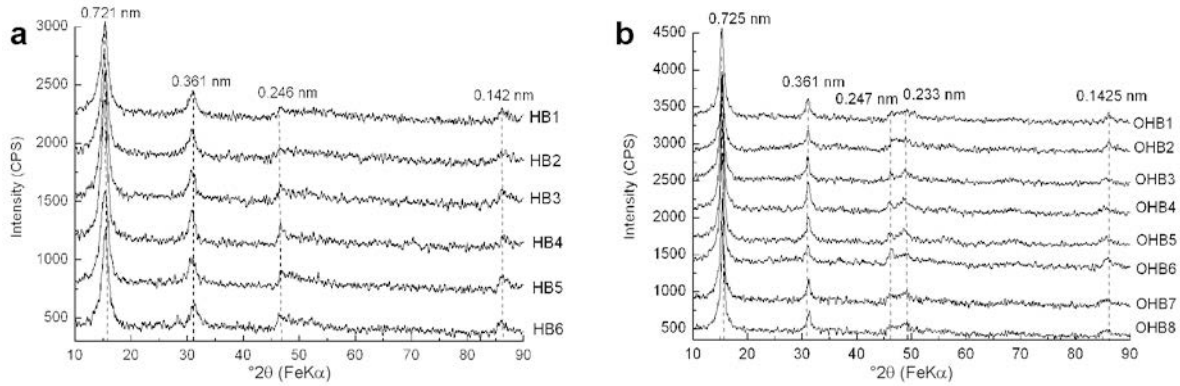

Figure 1. Powder XRD patterns of (a) acid-synthesized HB and (b) alkaline-synthesized OHB series birnessites with a range of average Mn oxidation states.

polyethylene centrifuge tubes. A solid to liquid ratio of ~1.67 g/L was obtained and the Pb^{2+} concentrations ranged from 0 to 10 mM with an ionic strength of 0.1 during the reaction. The tubes were then capped and shaken for 24 h at 25±1ºC. The pH of the reaction system was maintained at 5.00±0.05 by hourly additions of NaOH or HNO_3 using a pH-stat technique, where the amounts of the HNO_3/NaOH solution added were recorded. Finally, the tubes were centrifuged at 22400 × g for 10 min in a J2-MC Super-speed refrigerated centrifuge (Beckman, America). The supernatants were collected and analyzed for Pb^{2+} and Mn^{2+} concentrations using a Varian AAS 240FS atomic absorption spectrometer, and for K^+ concentration with a flame spectrophotometer. The amounts of Pb^{2+} adsorbed and the amounts of Mn^{2+} and K^+ released during the whole adsorption process were obtained by comparison with a control group without any Pb^{2+} added. The amount of H^+ released was determined from the recorded additions of standard HNO_3/NaOH solutions. All measurements were performed in triplicate and averaged. No $PbCO_3$ precipitate should have formed during the Pb^{2+} adsorption experiments.

RESULTS

Characterization of the synthesized samples

Powder XRD patterns indicate that the synthetic birnessites are single phase (Figure 1). The HB acid-series birnessites have four characteristic peaks at 0.721, 0.361, 0.246, and 0.142 nm (Figure 1a). The OHB alkaline-series birnessites have five characteristic peaks at 0.725, 0.361, 0.247, 0.233, and 0.1425 nm (Figure 1b).

The Mn contents of the synthetic birnessites generally decreased with increases in AOS and the linear statistical correlation coefficient ($r = -0.9318$, $n = 14$, $p < 0.01$) was very significant (Table 1). The Mn contents of the HB-series birnessite ranged from 49.6 to 53.6 wt.% and were less than the OHB-series birnessites. Moreover, the HB-series AOS values ranged from 3.67 to 3.92, whereas, the OHB-series AOS values ranged from 3.49 to 3.89.

Although the AOS values for the birnessites prepared under acidic and alkaline conditions were different, the morphologies and particle sizes observed using TEM were similar. Differences in the AOS might result in differences in short-range or substructural characteristics of birnessites, such as the amount of vacant Mn octahedral sites and interlayer Mn^{2+} or Mn^{3+}, but the long-range structure indicated by XRD (Figure 1) and TEM (Figure 2) examination were not affected. The HB-series birnessites consisted of clusters of 100 to 200 nm spheroidal aggregates, consistent with the balls of needles described by McKenzie (1971). The balls, observed using HR-TEM, were actually randomly stacked aggregates of thin plates, as reported by Feng *et al.* (2007). The OHB-series birnessites consisted of 100 to 250 nm thin plates that were irregularly shaped along the (001) plane (Feng *et al.*, 2004).

Diffraction peaks of the (110) crystal plane for all birnessite samples were obtained using a two-peak Gaussian fit, which was calibrated using the 310 diffraction peak of rutile (Figure 3). The experimental diffraction peaks overlap the 110 and 113 diffraction peaks. A significant, negative linear correlation ($r = -0.9035$, $n = 14$, $p < 0.01$) was found between the birnessite AOS values

Table 1. The Mn content (wt.%) and AOS of all the samples.

HB series	Total Mn	AOS	OHB series	Total Mn	AOS
HB1	49.6	3.92	OHB1	50.0	3.89
HB2	50.5	3.91	OHB2	54.1	3.76
HB3	51.3	3.88	OHB3	53.5	3.63
HB4	51.6	3.84	OHB4	54.2	3.60
HB5	52.8	3.83	OHB5	54.5	3.60
HB6	53.6	3.67	OHB6	56.8	3.58
			OHB7	57.3	3.51
			OHB8	56.2	3.49

https://doi.org/10.1346/CCMN.2009.0570501 Published online by Cambridge University Press

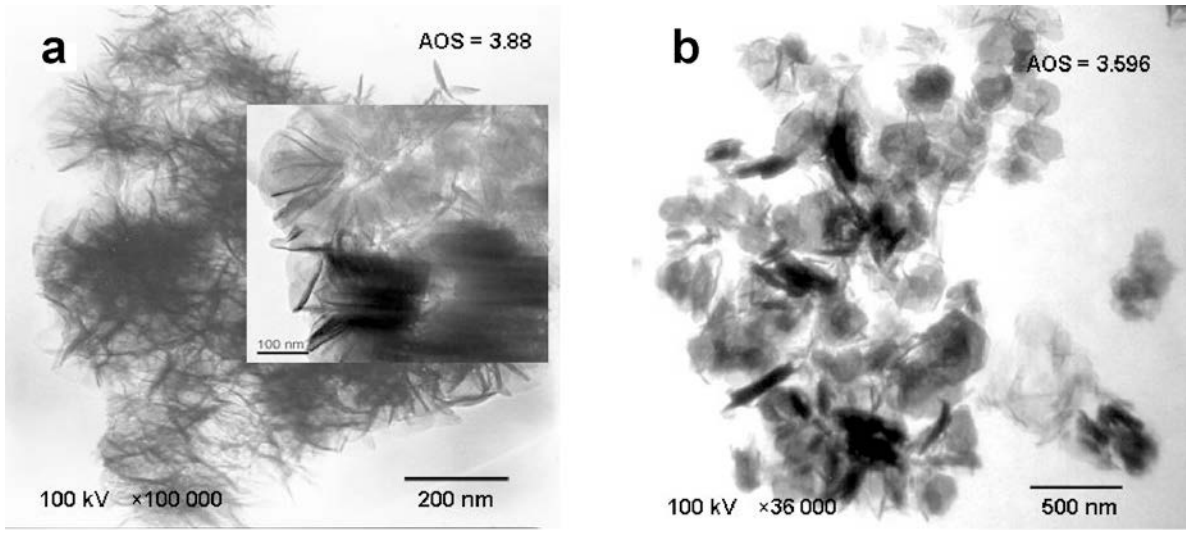

Figure 2. TEM images of the synthetic birnessites: (a) HB3; (b) OHB5.

and the d_{110} interlayer spacings derived from the Gaussian fit. This indicated that crystal structure distortion along (*hk*0) increased as birnessite AOS values increased and led to decreased (*hk*0) interlayer spacings. When AOS values increased from 3.49 to 3.92, the 110 interlayer spacing decreased from 0.1428 to 0.1416 nm (Table 1), indicating that the number of vacant structural sites increased with the increase in AOS values.

Isothermal adsorption of heavy metals by two series of birnessites

The similarly shaped Pb^{2+} adsorption isotherms (Figure 4) for the HB- and OHB-series birnessites could be assigned to L-type (Giles *et al.*, 1960). The amount of Pb^{2+} adsorbed initially increased sharply, leveled off, and then approached a maximum value as equilibrium Pb^{2+} concentrations increased. All the adsorption isotherms were fitted using the Langmuir non-linear model and the fitting parameters are listed in Table 2. The Langmuir equation is $Y = A_{max}KC/(1+KC)$, where Y is the amount adsorbed per unit weight (mmol/kg), A_{max} represents the maximum Pb^{2+} adsorption, C is the equilibrium Pb^{2+} concentration, and K is a constant related to adsorption energy as a function of adsorption enthalpy and temperature (Kinniburgh, 1986). The maximum Pb^{2+} adsorption increased from 1320 to 2457 mmol/kg (Table 2) as the

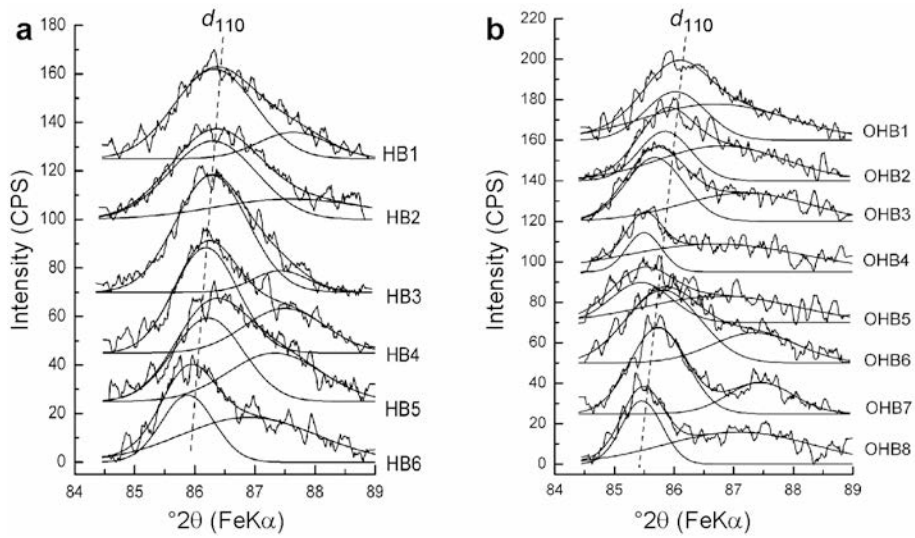

Figure 3. Crystal plane d_{110} XRD peaks for all the synthetic birnessites obtained by two-peak Gaussian fitting and calibrated using the rutile crystal plane d_{310} peak.

https://doi.org/10.1346/CCMN.2009.0570501 Published online by Cambridge University Press

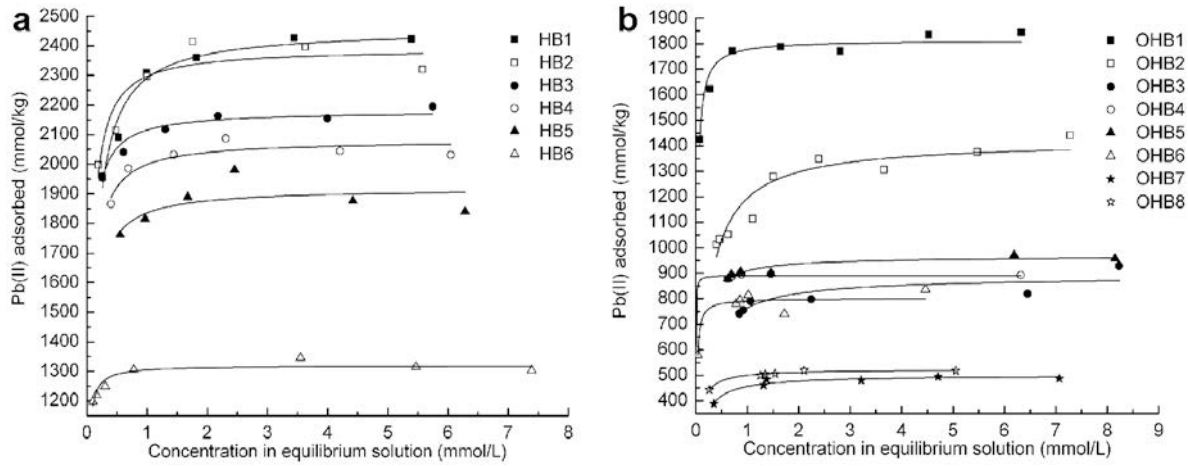

Figure 4. Adsorption of Pb^{2+} to the HB- and OHB-series birnessites at 25 ± 1ºC, pH = 5.00, I = 0.1 M $NaNO_3$, and 1.67 g/L birnessite.

AOS values of the HB-series of birnessites increased from 3.67 to 3.92 (Table 1), yielding a linear correlation (r = 0.9912, n = 6, p <0.01). Correlations between the maximum Pb^{2+} adsorption and AOS values of the OHB-series birnessites were also linear and very significant (r = 0.9907, n = 8, p <0.01).

Release of Mn^{2+}, H^+, and K^+ during Pb adsorption

The maximum amounts of Mn^{2+}, H^+, and K^+ released during Pb^{2+} adsorption varied with changes in birnessite AOS (Table 3). The AOS values for HB1, HB2, HB3, HB4, and HB5 birnessites were large and almost no Mn^{2+} was released. However, the HB6 birnessite had the smallest AOS value of the HB series and a maximum of 219 mmol/kg Mn^{2+} was released. The maximum Mn^{2+} release from the OHB series decreased from 218 to 55 mmol/kg (Table 3) as the AOS values increased from 3.49 to 3.89 (Table 1), indicating that the maximum Mn^{2+} release decreased as AOS values increased and that the Mn^{2+} release was similar for birnessites with comparable AOS values. Maximum H^+ release for the HB-series birnessites increased from 1735 to 2768 mmol/kg, maximum K^+ release increased from 273 to 1195 mmol/kg, and total maximum H^+, K^+, and Mn^{2+} release increased from 2228 to 3963 mmol/kg (Table 2) as AOS values increased from 3.67 to 3.92 (Table 1). Maximum H^+ release for the OHB-series birnessites increased from 573 to 2527 mmol/kg, maximum K^+ release increased from 89 to 608 mmol/kg, and total maximum H^+, K^+, and Mn^{2+} release increased from 876 to 3107 mmol/kg (Table 3) as AOS values increased from 3.49 to 3.89 (Table 1).

DISCUSSION

The relationship between the amount of Pb^{2+} adsorbed and the AOS

The d_{110} interlayer spacings of the birnessites decreased with increase in AOS (Figure 3, Table 1) which suggests that the number of vacant Mn octahedral sites increased as AOS increased. The positive correlation between maximum Pb^{2+} adsorption and AOS was linear and very significant (r = 0.9779, n = 14, p < 0.01), indicative of a positive correlation between Pb^{2+} adsorption and vacant Mn octahedral sites in birnessite. Based on the results of Villalobos *et al.* (2006),

Table 2. Langmuir parameters for adsorption of Pb^{2+} on all samples.

H-birnessite	Parameters			OH-birnessite	Parameters		
	A_{max} (mmol/kg)	K	r		A_{max} (mmol/kg)	K	r
HB1	2457	13.77	0.99	OHB1	1814	48.31	0.99
HB2	2391	24.33	0.99	OHB2	1420	5.313	0.99
HB3	2180	32.89	0.99	OHB3	887	6.238	0.99
HB4	2082	24.15	0.99	OHB4	892	555.6	0.99
HB5	1919	21.93	0.99	OHB5	966	16.13	0.99
HB6	1320	86.96	0.99	OHB6	802	74.63	0.99
				OHB7	500	10.31	0.99
				OHB8	524	20.75	0.99

https://doi.org/10.1346/CCMN.2009.0570501 Published online by Cambridge University Press

Table 3. The maximum amounts of Mn^{2+}, H^+, and K^+ released, the total maximum amounts of H^+ and K^+ released, and the total maximum amounts of Mn^{2+}, H^+, and K^+ released during Pb adsorption (mmol/kg).

Sample no.		Max. amount of Mn^{2+} released	Max. amount of H^+ released	Max. amount of K^+ released	Total max. amounts of H^+ + K^+ released	Total max. amounts of Mn^{2+} + H^+ +K^+ released
HB series	HB1	0	2768	1195	3963	3963
	HB2	0	2730	1103	3833	3833
	HB3	0	2749	872	3621	3621
	HB4	0	2514	811	3325	3325
	HB5	0	2654	414	3068	3068
	HB6	219	1735	273	2009	2228
OHB series	OHB1	55	2527	525	3052	3107
	OHB2	183	1720	317	2038	2220
	OHB3	193	892	608	1500	1693
	OHB4	218	980	375	1355	1573
	OHB5	207	966	299	1265	1472
	OHB6	216	1056	89	1177	1393
	OHB7	143	573	160	733	876
	OHB8	77	745	130	875	952

$(H^+,K^+)(Mn^{2+},Mn^{3+})_{tc}[Mn^{3+}_d,Mn^{4+}_e,\square_f]O_2{\cdot}nH_2O$ can be assigned as the general chemical formula of the birnessite samples, where interlayer species are written to the left of the square brackets, tc refers to interlayer Mn in triple corner-sharing positions above or below vacant Mn octahedral sites ($\square$) in the layers (enclosed in square brackets), and O_2 on the right refers to the O in the layers. Because the radius of Pb^{2+} (0.133 nm) is much larger than that of Mn^{3+} (0.066 nm) and Mn^{4+} (0.06 nm), it is impossible for Pb^{2+} to displace structural Mn^{3+} or Mn^{4+} and occupy the sites of the structural Mn. Therefore, Mn^{2+} released during the adsorption of Pb^{2+} derived mostly from the interlayer Mn^{2+} or Mn^{3+} located above or below vacant Mn octahedral sites (Matocha *et al.*, 2001). The HB1, HB2, HB3, HB4, and HB5 birnessites released almost no Mn^{2+}, which suggests that almost no interlayer Mn^{2+} or Mn^{3+} was present (*i.e.* the tc value $\approx$ 0). Some interlayer Mn^{2+} and Mn^{3+} might account for the small HB6 birnessite AOS value with a maximum release of 219 mmol/kg Mn^{2+} during Pb^{2+} adsorption. The numbers of vacant octahedral sites decreased in the HB1 to HB6 birnessites as d_{110} spacings increased (*i.e.* the f value decreased). A likely explanation is that Mn^{3+} quantities (*i.e.* the d value) increased by filling vacant sites as the AOS decreased and the quantity of more stable Mn^{4+} (*i.e.* the e value) remained nearly constant. In this case, the structural Mn content (*i.e.* the sum of d and e) increased from HB1 to HB6. This caused a decrease in net negative charge of the structure, which is the difference between the negative charges contributed by the oxygen framework and the positive charges contributed by structural Mn cations. The cation exchange capacity, which is closely related to net structural charge, also decreased and resulted in a decreased Pb^{2+} adsorption capacity. The d_{110} spacings of the OHB1 to OHB8 birnessites tended to increase as AOS decreased, which suggests a corresponding decrease in the number of vacant Mn octahedral sites. On the other hand, Mn^{2+} released from the OHB birnessites tended to increase from OHB1 to OHB8 during Pb^{2+} adsorption, suggesting an increased number of interlayer Mn^{2+} and Mn^{3+} which is one reason for an AOS decrease. During Pb^{2+} adsorption, Mn^{3+} displaced by Pb^{2+} adsorption would probably disproportionate into Mn^{2+} and Mn^{4+}. The Mn^{4+} released could enter the birnessite structure, fill vacant sites, and further decrease the number of vacant sites available for Pb^{2+} adsorption. This is similar to Co^{2+} oxidation by the phyllomanganate mineral, buserite (Manceau *et al.*, 1997), where the Co^{3+} that is produced can fill vacant sites. As a result, disproportionation of displaced Mn^{3+} from birnessites with smaller AOS values, such as OHB6, would tend to yield greater quantities of Mn^{4+} to fill vacant sites. For birnessites with smaller AOS values and cation exchange capacities, these factors result in fewer site vacancies and, therefore, a smaller maximum Pb^{2+} adsorption capacity. In contrast, birnessites with greater AOS values and more octahedral Mn site vacancies would lead to a greater Pb^{2+} adsorption capacity. Therefore, the number of structural Mn site vacancies in birnessites is probably responsible for determining the Pb^{2+} adsorption capacity.

Maximum Pb^{2+} adsorption differed significantly for birnessites with similar AOS values for the HB-series and OHB-series birnessites. For example, the HB3 sample AOS was 3.88 and the OHB1 sample AOS was 3.89, but the maximum Pb^{2+} adsorption was 2180 mmol/kg for HB3 and 1814 mmol/kg for OHB1 (Table 1). Great differences in the number of Mn^{3+} located above or below vacant sites and different crystal systems might explain the differences in Pb^{2+} adsorption for the HB and OHB samples.

https://doi.org/10.1346/CCMN.2009.0570501 Published online by Cambridge University Press

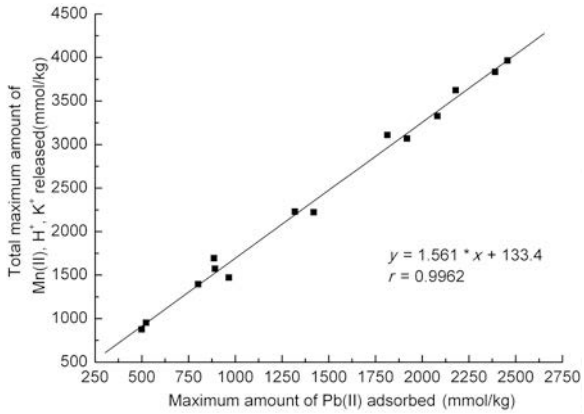

Figure 5. Linear correlation between the maximum Pb^{2+} adsorption and maximum total release of Mn^{2+}, H^+, and K^+ by the 14 synthetic birnessites.

Relationship between the amount of Mn^{2+}, H^+, and K^+ released during adsorption of Pb^{2+} and the AOS

The positive linear correlation (r = 0.9962, n = 14, $p < 0.01$) between the amounts of Mn^{2+}, H^+, and K^+ released and the amounts of Pb^{2+} adsorbed was very significant (Figure 5). This suggests a relationship between vacant Mn structural sites in birnessite and adsorption of Pb^{2+} (Lanson *et al.*, 2002b; Manceau *et al.*, 2002). The amounts of Mn^{2+}, H^+, and K^+ released during Pb^{2+} adsorption were, therefore, mostly derived from interlayer exchangeable cations attached to vacant sites (Gaillot *et al.*, 2003; Lanson *et al.*, 2000; Matocha *et al.*, 2001).

Birnessite samples with smaller AOS values (3.49–3.76, Table 1) released more Mn^{2+} (Table 3) than birnessites with larger AOS values (3.83–3.92). Conversely, birnessite samples with larger AOS values released more H^+ and K^+. Birnessites with large AOS values had larger Mn^{4+} contents, smaller Mn^{2+} and Mn^{3+} contents, and more site vacancies available for adsorption of heavy metals.

CONCLUSIONS

The average oxidation state of Mn in birnessites apparently reflects the number of vacant structural Mn sites, which accounts for Pb^{2+} adsorption. The Pb^{2+} adsorption capacity of birnessites is positively correlated with the average oxidation state of Mn and negatively correlated with the d_{110} spacings. The correlation between greater Pb^{2+} adsorption and average oxidation state of Mn in birnessites suggests that the number of vacant sites increases with increase in the average oxidation state of Mn. The number of vacant Mn structural sites probably, therefore, determines the Pb^{2+} adsorption capacity.

ACKNOWLEDGMENTS

The authors are grateful to Matthew Siebecker and Prof. Huada Daniel Ruan for reviewing the final draft of this paper. They thank the National Natural Science Foundation of China (Grant No. 40471070) for financial support of this research, and the Foundation for the Author of National Excellent Doctoral Dissertation of the PR of China (No. 200767). Constructive remarks and comments by the Associate Editor and three anonymous reviewers helped to improve this paper.

REFERENCES

Appelo, C.A.J. and Postma, D. (1999) A consistent model for surface complexation on birnessite (-MnO_2) and its application to a column experiment. *Geochimica et Cosmochimica Acta*, **63**, 3039–3048.

Bailey, S.W. (1966) The status of clay mineral structures. *Clays and Clay Minerals*, **14**, 1–23.

Burns, R.G. (1976) The uptake of cobalt into ferromanganese nodules, soils, and synthetic manganese (IV) oxides. *Geochimica et Cosmochimica Acta*, **40**, 95–102.

Drits, V.A., Silvester, E., Gorshkov, A.I., and Manceau, A. (1997) Structure of synthetic monoclinic Na-rich birnessite and hexagonal birnessite; I. Results from X-ray diffraction and selected-area electron diffraction. *American Mineralogist*, **82**, 946–961.

Feng, X.H., Liu, F., Tan, W.F., and Liu, X.W. (2004) Synthesis of birnessite from the oxidation of Mn^{2+} by O_2 in alkali medium: Effects of synthesis conditions. *Clays and Clay Minerals*, **52**, 240–250.

Feng, X.H., Zhai, L.M., Tan, W.F., Liu, F., and He, J.Z. (2007) Adsorption and redox reactions of heavy metals on synthesized Mn oxide minerals. *Environmental Pollution*, **147**, 366–373.

Gaillot, A.C., Flot, D., Drits, V.A., Manceau, A., Burghammer, M., and Lanson, B. (2003) Structure of synthetic K-rich birnessite obtained by high-temperature decomposition of $KMnO_4$. I. Two-layer polytype from 800ºC experiment. *Chemistry of Materials*, **15**, 4666–4678.

Giles, C.H., MacEwan, T.H., Nakhwa, S.N., and Smith, D. (1960) Studies in adsorption Part XI. A system of classification of solution adsorption isotherms and its use in diagnosis of adsorption mechanisms and in the measurement of the specific surface area of solids. *Journal of Chemical Society*, **3**, 3973–3993.

Golden, D.C., Chen, C.C., and Dixon, J.B. (1987) Transformation of birnessite to buserite, todorokite, and manganite under mild hydrothermal treatment. *Clays and Clay Minerals*, **35**, 271–280.

Kijima, N., Yasuda, H., Sato, T., and Yoshimura, Y. (2001) Preparation and characterization of open tunnel oxide [alpha]-MnO_2 precipitated by ozone oxidation. *Journal of Solid State Chemistry*, **159**, 94–102.

Kinniburgh, D.G. (1986) General purpose adsorption isotherms. *Environmetal Science & Technology*, **20**, 895–904.

Lanson, B., Drits, V.A., Silvester, E., and Manceau, A. (2000) Structure of H-exchanged hexagonal birnessite and its mechanism of formation from Na-rich monoclinic buserite at low pH. *American Mineralogist*, **85**, 826–838.

Lanson, B., Drits, V.A., Feng, Q., and Manceau, A. (2002a) Structure of synthetic Na-birnessite: Evidence for a triclinic one-layer unit cell. *American Mineralogist*, **87**, 1662–1671.

Lanson, B., Drits, V.A., Gaillot, A.-C., Silvester, E., Plançon, A., and Manceau, A. (2002b) Structure of heavy-metal sorbed birnessite: Part 1. Results from X-ray diffraction. *American Mineralogist*, **87**, 1631–1645.

Luo, J. and Suib, S.L. (1997) Preparative parameters, magnesium effects, and anion effects in the crystallization of birnessites. *Journal of Physical Chemistry B*, **101**, 10403–10413.

Manceau, A. and Charlet, L. (1992) X-ray absorption spectroscopic study of the sorption of Cr(III) at the oxide-water

interface: I. Molecular mechanism of Cr(III) oxidation on Mn oxides. *Journal of Colloid and Interface Science*, **148**, 425–442.

Manceau, A., Drits, V.A., Silvester, E., Bartoli, C., and Lanson, B. (1997) Structural mechanism of Co^{2+} oxidation by the phyllomanganate buserite. *American Mineralogist*, **82**, 1150–1175.

Manceau, A., Lanson, B., and Drits, V. A. (2002) Structure of heavy metal sorbed birnessite. Part III: Results from powder and polarized extended X-ray absorption fine structure spectroscopy. *Geochimica et Cosmochimica Acta*, **66**, 2639–2663.

Matocha, C.J., Elzinga, E.J., and Sparks, D.L. (2001) Reactivity of Pb(II) at the Mn(III,IV) (oxyhydr)oxide-water interface. *Environmetal Science & Technology*, **35**, 2967–2972.

McKenzie, R.M. (1971) The synthesis of birnessite, cryptomelane, and some other oxides and hydroxides of manganese. *Mineralogical Magazine*, **38**, 493–502.

McKenzie, R.M. (1980) The adsorption of lead and other heavy metals on oxides of manganese and iron. *Australian Journal of Soil Research*, **18**, 61–73.

O'Reilly, S.E. and Hochella, M.F. (2003) Lead sorption efficiencies of natural and synthetic Mn and Fe-oxides. *Geochimica et Cosmochimica Acta*, **67**, 4471–4487.

Peacock, C.L. and Sherman, D.M. (2007) Sorption of Ni by birnessite: Equilibrium controls on Ni in seawater. *Chemical Geology*, **238**, 94–106.

Post, J.E. (1999) Manganese oxide minerals: Crystal structures and economic and environmental significance. *Proceedings of the National Academy of Sciences of the United States of America*, **96**, 3447–3454.

Post, J.E. and Veblen, D.R. (1990) Crystal structure determinations of synthetic sodium, magnesium, and potassium birnessite using TEM and the Rietveld method. *American Mineralogist*, **75**, 477–489.

Tu, S., Racz, G.J., and Goh, T. B. (1994) Transformations of synthetic birnessite as affected by pH and manganese concentration. *Clays and Clay Minerals* **42**, 321–330.

Villalobos, M., Toner, B., Bargar, J., and Sposito, G. (2003) Characterization of the manganese oxide produced by *pseudomonas putida* strain MnB1. *Geochimica et Cosmochimica Acta*, **67**, 2649–2662.

Villalobos, M., Bargar, J., and Sposito, G. (2005) Mechanisms of Pb(II) sorption on a biogenic manganese oxide. *Environmetal Science & Technology*, **39**, 569–576.

Villalobos, M., Lanson, B., Manceau, A., Toner, B., and Sposito, G. (2006) Structural model for the biogenic Mn oxide produced by *Pseudomonas putida*. *American Mineralogist*, **91**, 489–502.

Webb, S.M., Tebo, B.M., and Bargar, J.R. (2005) Structural characterization of biogenic Mn oxides produced in seawater by the marine *bacillus sp.* strain SG-1. *American Mineralogist*, **90**, 1342–1357.

(*Received 20 June 2008; revised 3 February 2009; Ms. 0174; A.E. W. Jaynes*)